NACA RM E54J26

RESEARCH MEMORANDUM

THRUST AND DRAG CHARACTERISTICS OF SIMULATED VARIABLE-SHROUD NOZZLES WITH HOT AND COLD PRIMARY FLOWS AT SUBSONIC AND SUPERSONIC SPEEDS

By Andrew Beke and Paul C. Simon

Lewis Flight Propulsion Laboratory
Cleveland, Ohio

NATIONAL ADVISORY COMMITTEE
FOR AERONAUTICS

WASHINGTON

February 18, 1955

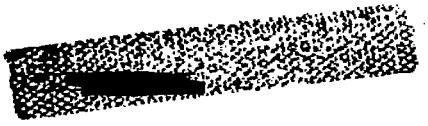

NATIONAL ADVISORY COMMITTEE FOR AERONAUTICS

RESEARCH MEMORANDUM

THRUST AND DRAG CHARACTERISTICS OF SIMULATED VARIABLE-SHROUD NOZZLES WITH HOT AND COLD PRIMARY FLOWS AT SUBSONIC AND SUPERSONIC SPEEDS

By Andrew Beke and Paul C. Simon

SUMMARY

An experimental investigation of a series of fixed-geometry exhaust nozzles which simulated a variable exit was conducted in the Lewis 8- by 6-foot supersonic wind tunnel at Mach numbers of 0, 0.6, 1.5, 1.7, and 2.0. The studies included long- and short-shroud configurations.

Gross thrust performance of the long-shroud exit configurations was considerably better than the performance of the short-shroud configurations. Thrusts of the long-shroud nozzle, or ejector, characteristically increased with secondary weight flow, whereas the thrusts of the short-shroud nozzle remained constant and about equal in value to that of an ideal sonic nozzle. Effect of free-stream Mach number on the thrusts appeared to be negligible.

Thrust performance analysis for flight Mach numbers from 0.6 to 2.0 at 35,000-feet altitude indicated that the long-shroud configuration had a 4 to 8 percent higher net thrust than the short-shroud configuration. Thrust ratios for the long-shroud configurations were slightly better than the thrust ratio for a variable ideal convergent-divergent nozzle below a Mach number of 1.3; above this speed, the thrust ratios of the long-shroud nozzle were below that for the ideal nozzle and remained fairly constant at a value of about 1.07.

The external pressure drag of the simulated variable shrouds amounted to a thrust force of about 2 percent of an ideal convergent-nozzle net thrust at the subsonic speed and diminished to approximately zero at a Mach number of 2.0.

INTRODUCTION

The use of ejectors for thrust augmentation has been established in several quiescent-air studies and in limited flight tests (refs. 1 to 3).

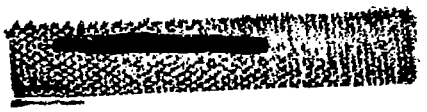

Knowledge, however, is needed of the comparative performance of long- and short-shroud nozzles and of the characteristic operation of a variable exit over given flight conditions. As part of a general program on jet-engine-exit configurations being conducted in the Lewis 8- by 6-foot supersonic wind tunnel, a series of fixed-geometry exit configurations having long and short shrouds and simulating a variable iris-type nozzle were tested on a typical supersonic airplane model in order to determine the effects of shroud length on thrust performance. Since previous experimental studies have been restricted to quiescent-air tests and since data on the drag penalty associated with shroud extensions are limited, one of the main purposes of this investigation is to establish the effects of free-stream Mach number on jet thrust and shroud drags.

Pumping characteristics of these configurations have been reported in references 4 and 5, and this report presents the gross and net thrust performance and the attendant shroud drags. The experiments were conducted over a wide range of primary-nozzle pressure ratio and over secondary weight-flow ratios ranging up to 10 percent of the primary-nozzle air flow at free-stream Mach numbers of 0, 0.6, 1.5, 1.7, and 2.0.

SYMBOLS

The following symbols are used in this report:

A	area, sq ft
A_{max}	fuselage maximum cross-sectional area, 0.336 sq ft
A_s/A_b	shroud-area ratio (ratio of cross-sectional areas at ends of shroud and boattail, respectively)
C_D	shroud external pressure drag coefficient, D/q_0A_{max}
C_f	primary-nozzle mass-flow coefficient, $W_p/W_{p,i}$
C_p	pressure coefficient, $\frac{p - p_0}{q_0}$
D	drag, lb
d_b	diameter at end of boattail, 4.70 in.
F	thrust, lb
f/a	fuel-air ratio
g	acceleration due to gravity, 32.2 ft/sec^2

[redacted]

M	Mach number
P	total pressure, lb/sq ft
p	static pressure, lb/sq ft
q	dynamic pressure, $\frac{\gamma}{2} pM^2$, lb/sq ft
T	total temperature, $^{\circ}R$
V	velocity, ft/sec
W	weight flow, lb/sec
x	longitudinal distance from end of boattail, in. (positive downstream and negative upstream)
λ	rate of change of shroud drag coefficient with nozzle pressure ratio, $\frac{d(C_D)}{d(P_p/p_0)}$
ω	$\frac{\text{secondary weight flow}}{\text{primary weight flow}}, \frac{W_s}{W_p}$
τ	$\frac{\text{secondary total temperature}}{\text{primary total temperature}}, \frac{T_s}{T_p}$
φ	shroud external half-angle, deg
γ	ratio of specific heats

Subscripts:

b	boattail
c	convergent
c-d	convergent-divergent
ej	ejector
G	gross
i	ideal
n	net

[redacted]

p primary

s secondary

0 free-stream conditions

APPARATUS AND PROCEDURE

The apparatus used in this jet-exit investigation is represented schematically in figure 1. Air from an external high-pressure supply line was throttled by means of the control valve to any desired operating pressure and preheated to about 600° to 800° R to prevent condensation effects in the nozzle. The air was measured with a standard A.S.M.E. sharp-edged orifice mounted ahead of the control valve and entered the model reservoir chamber through two hollow support struts which simulated the airplane wing. The preheater fuel flow was measured with a rotameter.

A sketch of the model afterbody with the location of primary and secondary air inlets, the reservoir chambers, and afterbody cross-sectional characteristics is shown in figure 2. The temperature of the reservoir chamber air was measured as it entered the model and was approximately equal to the preheated value. For hot flow, the temperature of the primary air was varied from 1200° to approximately 3000° R by means of heat addition from a ram-jet combustor within the model. Secondary air flow was controlled by means of the perforated annulus ring-type valve, which permitted various amounts of air to be bled from the main reservoir chamber to the secondary passage between the primary combustion chamber and the model skin. The secondary air temperature was equal to the preheated air temperature (600° to 800° R).

Details of the exit configurations showing pertinent physical dimensions and internal and external pressure instrumentation are shown in figures 3 and 4. The configurations in figures 3(a) and 4(a) are sized for the nonafterburning condition of a turbojet engine, while the remaining figures are for other simulated positions of a variable iris-type nozzle with tail-pipe conditions as indicated in table I. The reexpanding nozzle designed for an expansion ratio of 2.87 (figs. 3(c) and 4(c)) is an alternate design for the convergent primary nozzle of figures 3(d) and 4(d). All the configurations had smooth internal and external surfaces and were designed to simulate given exit-area requirements rather than to duplicate the actual sliding-leaf or iris-type nozzle surfaces.

The notation appearing below each configuration classifies the type of nozzle by defining the diameter ratio and spacing ratio, respectively, and is based on the exit diameter of the primary nozzle. Each primary

[redacted]

nozzle was investigated with a long and short shroud, as seen in figures 3(a) to (d) and 4(a) to (d), respectively. Also, in a few cases, alternate nozzles were used with approximately the same shrouds (figs. 3(c) and (d) and 4(c) and (d)).

Performance of the nozzle configurations was determined for a range of primary pressure ratio from 2 to about 12 for free-stream Mach numbers from zero to 2.0 at zero angle of attack. The secondary weight-flow ratios ranged from zero to approximately 10 percent of the primary-nozzle air flow, for the entire range of primary-nozzle temperature and pressure ratio. The flow coefficients of the primary nozzles were obtained from both static calibrations with the shroud removed and measurements during testing with shrouds in place. Nozzle pumping characteristics are reported in references 4 and 5 (configuration B).

In order to calculate the gross thrust from pressure instrumentation for primary flow temperatures of 600° to 800° R, the pumping characteristics of the configurations reported in references 4 and 5 have been used with the method of reference 6. For the long shroud (or ejector) the method essentially consists of determining the gross thrust at the shroud exit by calculating the primary and secondary gross thrust at the primary-nozzle exit plane from one-dimensional equations and introducing the momentum decrement due to internal pressures on the shroud wall. Frictionless flow along the shroud wall and a ratio of specific heats of 1.4 were assumed in these calculations. The momentum decrement due to the effect of shroud convergence was obtained by integration of the internal pressures on the shroud wall. The gross thrusts of the short-shroud configurations were computed in a similar manner; that is, the gross thrusts of the primary exit and the secondary exit were obtained and, in effect, these thrusts constitute the jet thrust inasmuch as there are no shroud wall forces. The calculated gross thrust conforms to the conventional jet-thrust definition and is the difference between the total momentum of the jet stream and the force exerted by the ambient pressure on the stream cross-sectional area. In order to establish the thrust for higher primary air-flow temperatures (1200° to 3000° R), an iteration process was used in conjunction with the nozzle mass-flow calibrations for nozzle temperatures of 600° to 800° R to determine the ratio of specific heats.

Since the gross-thrust ratio is not indicative of the installed propulsive performance of these nozzles, the net thrust was obtained by subtracting the ram drag of the primary and secondary air flow from the gross thrust. The following equation was used in these calculations:

$$\left(\frac{F_{ej}}{F_{i,c}}\right)_n = \frac{\left(\frac{F_{ej}}{F_{i,c}}\right)_G (F_{i,c})_G - \frac{W_p}{g} V_0 \left\{ \frac{1}{(1 + f/a)} + \omega\sqrt{\tau}\sqrt{\frac{T_p}{T_s}} \right\}}{(F_{i,c})_G - \frac{W_p}{g} V_0 \frac{1}{(1 + f/a)}} \qquad (1)$$

[redacted]

where $(F_{i,c})_G = \frac{W_p}{g} V_i + (p_i - p_0)A_p C_f$. It was assumed that the gross thrust ratios and the temperature-corrected weight-flow ratios were independent of the primary-nozzle temperature. The primary-nozzle temperature was scheduled according to table I, and the secondary-nozzle total temperature was assumed to be the stagnation temperature of the free stream for standard NACA conditions at an altitude of 35,000 feet.

The shroud external-pressure-drag coefficients were obtained from integration of the external pressure distributions on the shrouds. The annular opening which existed between the shroud and fuselage boattail was sealed during operation of the ejector configurations. The character or effects of the small amount of air flow issuing from the opening could not be ascertained during short-shroud nozzle operation.

RESULTS AND DISCUSSION

Experimental data for the mass-flow coefficients, the gross-thrust characteristics, and the external-shroud pressure drags of all the configurations for a range of primary-nozzle pressure ratio, for free-stream Mach numbers of zero to 2.0, and at zero angle of attack are presented in figures 5 to 8 and 14 and 15.

Flow Coefficients

Primary-nozzle mass-flow coefficients are shown for secondary weight flows of 1 and 10 percent in figure 5. In general, the values of the coefficients were nearly 1.00 for the entire range of primary pressure ratio. For the ejector configurations, increased secondary flow appears to decrease the primary flow coefficients slightly (figs. 5(a), (b), and (d)). This effect was also observed in reference 7, which indicates decreases of flow coefficient up to 15 percent for increases in secondary weight-flow ratios of approximately 40 percent. No appreciable effect of free-stream Mach number on the flow coefficients is indicated for the entire range of nozzle pressure ratio.

Thrust Characteristics

Ejector thrust ratios (ratio of nozzle thrust to the thrust of an ideal sonic nozzle discharging the actual nozzle mass flow) characteristically increased with increased secondary weight-flow ratio and primary-nozzle pressure ratio (fig. 6). Gross thrusts of from 5 to 15 percent greater than ideal sonic nozzle thrusts were obtained with 10-percent secondary weight flow for the range of pressure ratio investigated. No Mach number effects on thrust performance are apparent from the data.

For the short-shroud configurations, increases of secondary weight flow did not produce pronounced increases in thrust (fig. 7). The thrust values did not exceed the ideal convergent-nozzle thrust by more than 2 percent for weight-flow ratios up to 3 percent; at the maximum weight flows, the thrust ratios were not greater than 1.03. Also, as found for the ejectors or long shrouds, free-stream Mach number had no effect upon the thrusts of the short-shroud configurations.

At any arbitrary pressure ratio it can be seen that the rate of change of thrust with secondary weight flow is greater for the long shrouds than for the short shrouds and that the performance is better for all configurations with long shrouds. It should be pointed out that the full-scale performance of these nozzles may be somewhat lower than indicated, because the configurations used in these tests duplicate only nozzle-area size and in no way reflect the penalty which may result from internal flow losses due to leaf actuators and irregular flow surfaces of full-scale exits. For the range of temperature investigated, the use of corrected secondary weight-flow ratio appeared to correlate the thrust data fairly well.

Figure 8 is presented for convenience in converting the thrust ratios presented in figure 6 to thrust based on an ideal reexpanding nozzle. The curves were computed for specific-heat ratios of 1.3 and 1.4, and are for flow coefficients of 1.0.

Flight Performance Analysis of Data

In order to evaluate the flight performance of the experimental thrust data presented in figures 6 and 7, assumed turbojet-engine operating nozzle pressure ratios for a range of flight Mach number, an altitude of 35,000 feet, and for conditions with and without afterburning are presented in figure 9.

Gross-thrust ratios for the nozzles are plotted at the assumed engine operating conditions in figures 10 and 11. Net thrusts were determined from equation (1) for the assumed flight conditions. Afterburning performance at a free-stream Mach number of 0.6 was obtained by interpolating the ejector data at the attendant spacing ratio for the engine match-point exit area. This flight condition was selected to illustrate the performance of the nozzle sizes tested rather than to satisfy typical aircraft operational characteristics. In nearly all cases the long-shroud, or ejector, net-thrust ratios increased with secondary weight flow and indicated better performance than the short-shroud configurations. Larger gross and net thrusts were obtained with afterburning at a free-stream Mach number of 0.6 (fig. 11(b)) because of the decreased spacing ratio associated with the change in operation from nonafterburning to afterburning nozzle positions. Temperature effects on gross-thrust ratios, reported in references 3 and 8, showed increased thrust values with increased tail-pipe temperature. Inasmuch as the gross-thrust data

of figure 6 do not reflect this same trend (the ratios are approximately the same for the entire temperature range), the results presented herein are somewhat conservative estimates of the large-scale high-temperature performance of these exit configurations.

Since the thrust is affected by secondary weight flow, two schedules of the variation of secondary weight flow with Mach number were determined by matching fixed-geometry inlet characteristics with the pumping characteristics of these nozzles (refs. 4 and 5). These data are presented in figure 12. A low-recovery inlet (boundary-layer scoop) sized at a free-stream Mach number of 2.0 was used to obtain schedule 1 and a high-recovery inlet sized subsonically was used for schedule 2. Low-recovery inlet data were reported in reference 9 and in unpublished data from the Lewis 8- by 6-foot supersonic tunnel, and data for the high-performance inlet were found in references 10 and 11. Schedule 1 was selected as a means of comparing the long- and short-shroud net thrusts, while schedule 2 is presented as a more practical cooling air-flow supply. The decreasing weight flow in the subsonic region for schedule 1 was due to inlet pressure-recovery limitations.

3434

Results of using the net thrusts of figures 10 and 11, the weight-flow schedules, and the flight plan are shown in figure 13. Performance of the ejector with schedule 1 was better than that of the short-shroud nozzle by at least 4 percent at subsonic speeds and by about 8 percent at supersonic speeds. The thrust ratios for schedule 1 are somewhat low because the gross thrust of the secondary air flow was charged with the ram drag of free-stream air instead of the ram drag of the fuselage boundary-layer air.

For a range of presumably practical secondary weight flow (schedule 2), the thrust ratios for the long-shroud nozzle were 3 to 7 percent greater than the ideal sonic thrust value. Therefore, the long-shroud nozzle performance was better than that of the short-shroud exits for the range of flight conditions and secondary air flows considered. The variable-exit ejector displayed slightly better performance than a variable ideal convergent-divergent nozzle up to a free-stream Mach number of 1.3. Between free-stream Mach numbers of 1.3 and 2.0, the ideal nozzle thrust ratio increased up to 1.145, while the variable-exit ejector remained nearly constant at a value of about 1.07 (fig. 13).

Shroud Drag

Instrumentation for external afterbody pressure was limited to the nozzle shroud during this investigation and thus represents only a portion of the afterbody drag that may be affected by nozzle pressure ratio. The shroud external-pressure-drag coefficients C_D are presented in figures 14 and 15 for a range of primary pressure ratio P_p/p_0 and secondary weight-flow ratio $\omega\sqrt{\tau}$. The slopes λ of lines of constant $\omega\sqrt{\tau}$ are indicated on each graph and represent the rate of change of

change of shroud drag coefficient with primary-nozzle pressure ratio. The effect of increasing primary-nozzle pressure ratio on drag coefficient was to decrease the shroud pressure drag; the rate of change λ was more pronounced for the smaller area ratios A_s/A_b. The drag coefficients varied from a maximum negative value of -0.030 at Mach number 0.6 to a maximum positive value of 0.022 at Mach number 2.0. These drag values can represent as much as 6 percent of a typical airplane drag. Reductions in shroud-area ratio produced decreases in shroud pressure drag at the subsonic speed and increases in drag at supersonic speeds. For configurations designed to meet the scheduled flight and engine conditions described in figure 9, the shroud pressure drag coefficients varied from a minimum of -0.025 at Mach number 0.6 (configuration 1.16-0.494, fig. 14(a)) to zero at Mach number 2.0 (configuration 1.12-0.123, fig. 14(c)). This thrust force at Mach number 0.6 amounts to 2 percent of ideal convergent-nozzle net thrust (without afterburning).

The pressure drags of the long shrouds are consistently lower than the drags of the corresponding short shrouds (same nozzle) at Mach number 0.6; this drag trend is associated with the fact that the long shrouds have characteristically greater projected areas. The long- and short-shroud nozzles have approximately equal drags at the supersonic speeds, since lengthening of the shroud adds very little projected area when the shroud is in the open position.

The influence of secondary weight-flow ratio on shroud drag appears to be negligible for the range tested (figs. 14 and 15), except for the configurations with small shroud-area ratios where there is a tendency for the drag to decrease slightly with increasing secondary weight flow.

The effect of increased jet-exit gas temperature on shroud pressure drag appears to be negligible.

Shroud external-pressure-coefficient distributions C_p are presented in figure 16 at free-stream Mach numbers of 0.6 and 2.0 for configurations 1.12-0.123 and 1.16-0.494. These configurations represent two extremes in shroud-area ratio (0.93 and 0.40) and shroud half-angle (1.5° and 15°). At both Mach numbers, a pressure drop occurred when the shroud angle was increased from 1.5° to 15°. At Mach number 2.0 the decrease in pressure level, as well as the increase in shroud projected area, caused an increase in drag coefficient as indicated on the figure; at the subsonic Mach number, the slight decrease in positive pressure coefficient as the shroud angle was increased was more than compensated for by the increase in projected area, resulting in a large decrease in drag.

The steeper boattail angle on the lower portion of the fuselage (fig. 2) resulted in consistently higher pressures on the bottom of the shroud, as can be seen in figure 17, where the pressure distribution on

the aft portion of the boattail is presented for the model without a shroud or nozzle and with the base covered. The pressure distributions on the shrouds of all the configurations tested did not indicate the presence of flow separation.

The pressure drag of the external surfaces of the fuselage boattail and nozzle shroud are uniquely influenced by the airplane forebody and wing-tail configuration as well as by the exiting jet flow (refs. 12 and 13). Also, at subsonic speeds, changes in shroud geometry affect a large upstream portion of the boattail (ref. 14). Therefore, the variations in shroud drag presented herein do not necessarily reflect the changes in total afterbody drag; the total afterbody-drag variations may conceivably differ in trend and magnitude from the shroud drags presented.

3434

SUMMARY OF RESULTS

An experimental investigation of long- and short-shroud exhaust-nozzle configurations was conducted in the Lewis 8- by 6-foot supersonic wind tunnel at free-stream Mach numbers of 0, 0.6, 1.5, 1.7, and 2.0 for a range of primary-nozzle pressure ratio and secondary weight flow. The following results were obtained:

1. Long shrouds, or ejectors, produced thrust ratios that were considerably higher than the thrust ratios of the short shrouds. Short-shroud exit thrusts were approximately that of an ideal sonic nozzle, while with 10 percent secondary weight flow the long-shroud nozzles, or ejectors, showed 5 to 15 percent improvement in thrust over the ideal sonic value.

2. The effect of free-stream Mach number on the thrust performance of the long- and short-shroud exits appeared to be negligible, and the use of corrected secondary weight-flow ratio correlated the thrusts fairly well.

3. Application of the experimental data to a turbojet engine indicated that the net thrust performance of the ejector was 4 to 8 percent better than that of the exit with a short shroud for free-stream Mach numbers of 0.6 to 2.0 at an altitude of 35,000 feet. The performance of the ejector was slightly better than that of a variable ideal reexpanding nozzle up to a free-stream Mach number of 1.3. Above this speed, the performance of the reexpanding nozzle was superior.

4. The external pressures acting on the simulated variable-exit shrouds produced a thrust force which amounted to about 2 percent of ideal convergent-nozzle net thrust at the subsonic speed and diminished to approximately zero at Mach number 2.0.

5. The drags of the long-shroud nozzles were consistently lower than the drags of the corresponding short-shroud nozzles at Mach number 0.6 and were approximately equal at Mach numbers from 1.5 to 2.0.

Lewis Flight Propulsion Laboratory
National Advisory Committee for Aeronautics
Cleveland, Ohio, November 12, 1954

3434

CR-2 back

REFERENCES

1. Greathouse, W. K., and Hollister, D. P.: Preliminary Air-Flow and Thrust Calibrations of Several Conical Cooling-Air Ejectors with a Primary to Secondary Temperature Ratio of 1.0. I - Diameter Ratios of 1.21 and 1.10. NACA RM E52E21, 1952.

2. Greathouse, W. K., and Hollister, D. P.: Preliminary Air-Flow and Thrust Calibrations of Several Conical Cooling-Air Ejectors with a Primary to Secondary Temperature Ratio of 1.0. II - Diameter Ratios of 1.06 and 1.40. NACA RM E52F26, 1952.

3. Rolls, L. Stewart, and Havill, C. Dewey: An Evaluation of Two Cooling-Air Ejectors in Flight at Transonic Speeds. NACA RM A54A05, 1954.

4. Allen, John L.: Pumping Characteristics for Several Simulated Variable-Geometry Ejectors with Hot and Cold Flow. NACA RM E54G15, 1954.

5. Vargo, Donald J.: Effects of Secondary-Air Flow on Annular Base Force of a Supersonic Airplane. NACA RM E54G28, 1954.

6. Huntley, S. C., and Yanowitz, Herbert: Pumping and Thrust Characteristics of Several Divergent Cooling-Air Ejectors and Comparison of Performance with Conical and Cylindrical Ejectors. NACA RM E53J13, 1954.

7. Gorton, Gerald C.: Pumping and Drag Characteristics of an Aircraft Ejector at Subsonic and Supersonic Speeds. NACA RM E54D06, 1954.

8. Greathouse, W. K.: Preliminary Investigation of Pumping and Thrust Characteristics of Full-Scale Cooling-Air Ejectors at Several Exhaust-Gas Temperatures. NACA RM E54A18, 1954.

9. Pennington, Donald B., and Simon, Paul C.: Internal Performance at Mach Numbers to 2.0 of Two Auxiliary Inlets Immersed in Fuselage Boundary Layer. NACA RM E53L28b, 1954.

[redacted]

10. Messing, Wesley E., and Acker, Loren W.: Transonic Free-Flight Drag Results of Full-Scale Models of 16-Inch-Diameter Ram-Jet Engines. NACA RM E52B19, 1952.

11. Nussdorfer, T., Wilcox, F., and Perchonok, E.: Investigation at Zero Angle of Attack of a 16-Inch Ram-Jet Engine in 8- by 6-Foot Supersonic Wind Tunnel. NACA RM E50L04, 1951.

12. Cortright, Edgar M., Jr., and Schroeder, Albert H.: Investigation at Mach Number 1.91 of Side and Base Pressure Distributions over Conical Boattails without and with Jet Flow Issuing from Base. NACA RM E51F26, 1951.

13. Englert, Gerald W., Vargo, Donald J., and Cubbison, Robert W.: Effect of Jet-Nozzle-Expansion Ratio on Drag of Parabolic Afterbodies. NACA RM E54B12, 1954.

14. Salmi, Reino J.: Experimental Investigation of Drag of Afterbodies with Exiting Jet at High Subsonic Mach Numbers. NACA RM E54I13, 1954.

[redacted]

TABLE I. - ASSUMED EXIT CONDITIONS AND FLIGHT SPEEDS FOR VARIOUS CONFIGURATIONS

[Altitude, 35,000 ft; standard NACA conditions]

Configuration	Primary total temperature, T_p, °R	Free-stream Mach number, M_O
1.16-0.494	[a]1400	0.6
1.39-0.09	↓	.6
1.27-(-0.10)	[b]3500	.6
1.14-0.214	↓	1.5
1.18-(-0.06)	↓	2.0
1.13-(-0.19)	↓	2.0
1.12-0.123	↓	2.0
1.16-0.133	↓	2.0
1.18-(-0.14)	↓	2.0

[a]No afterburning.

[b]Afterburning.

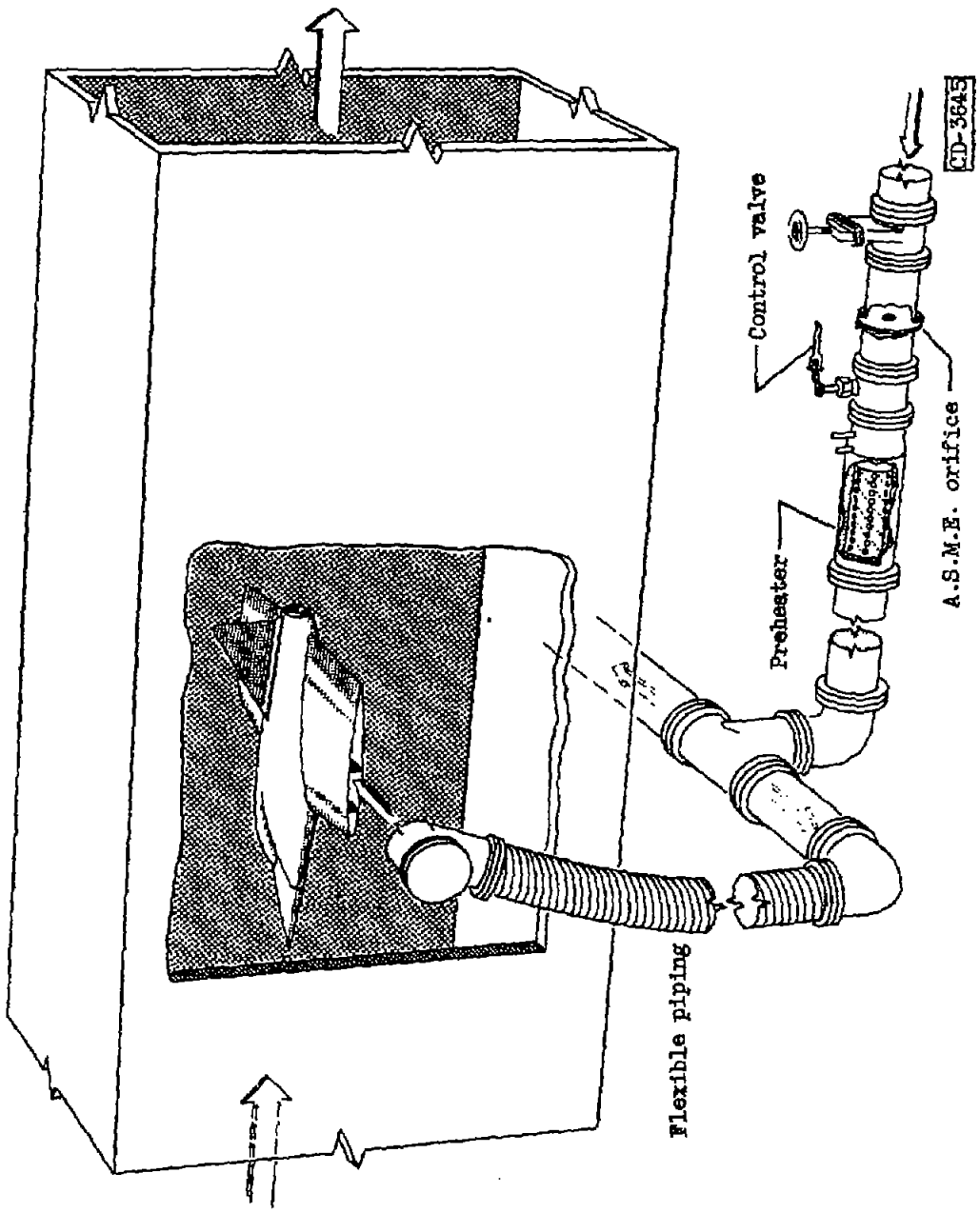

Figure 1. - Schematic diagram of jet-exit model installed in 8- by 6-foot supersonic tunnel.

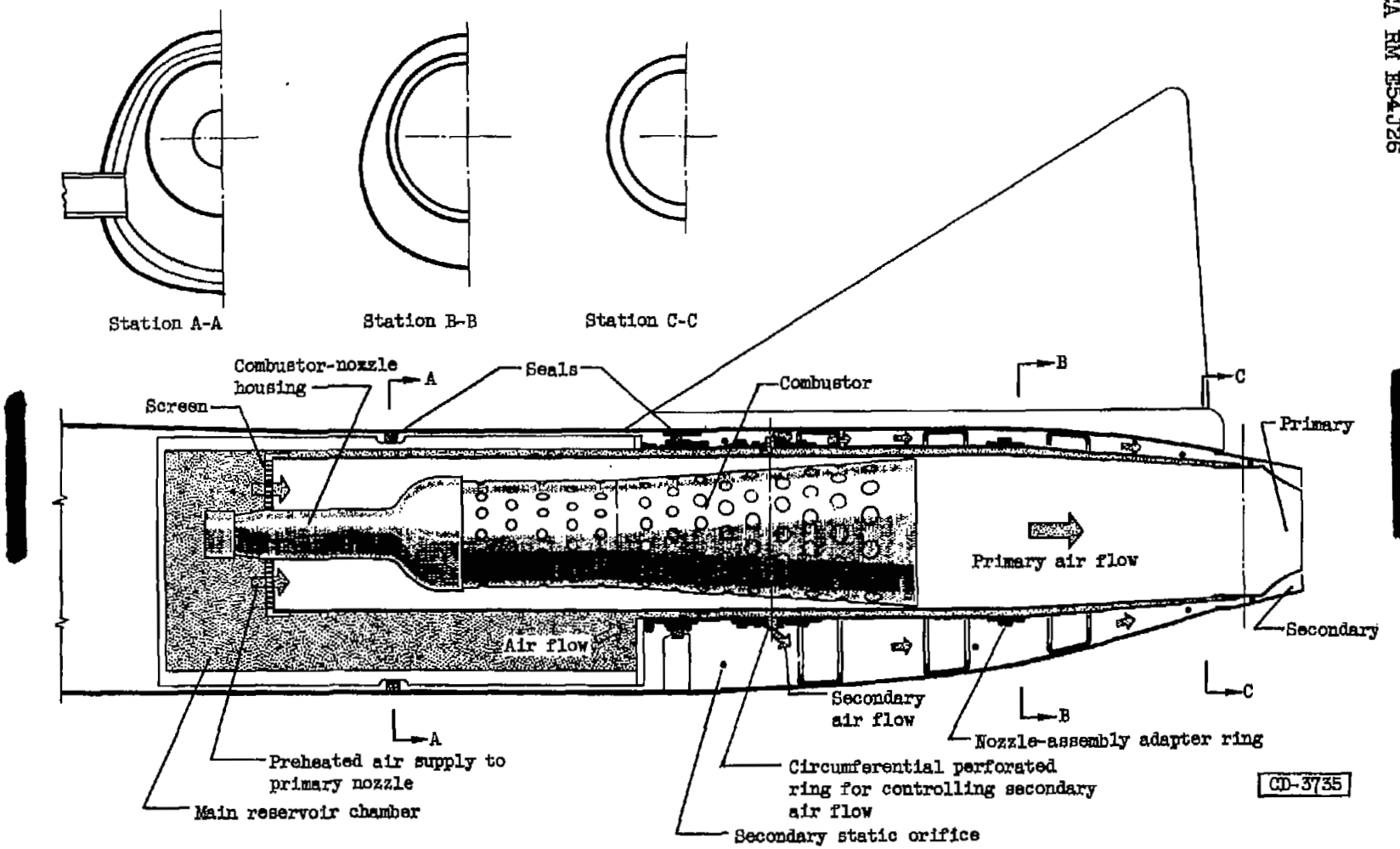

Figure 2. - Sketch of test model showing internal components and afterbody configuration characteristics.

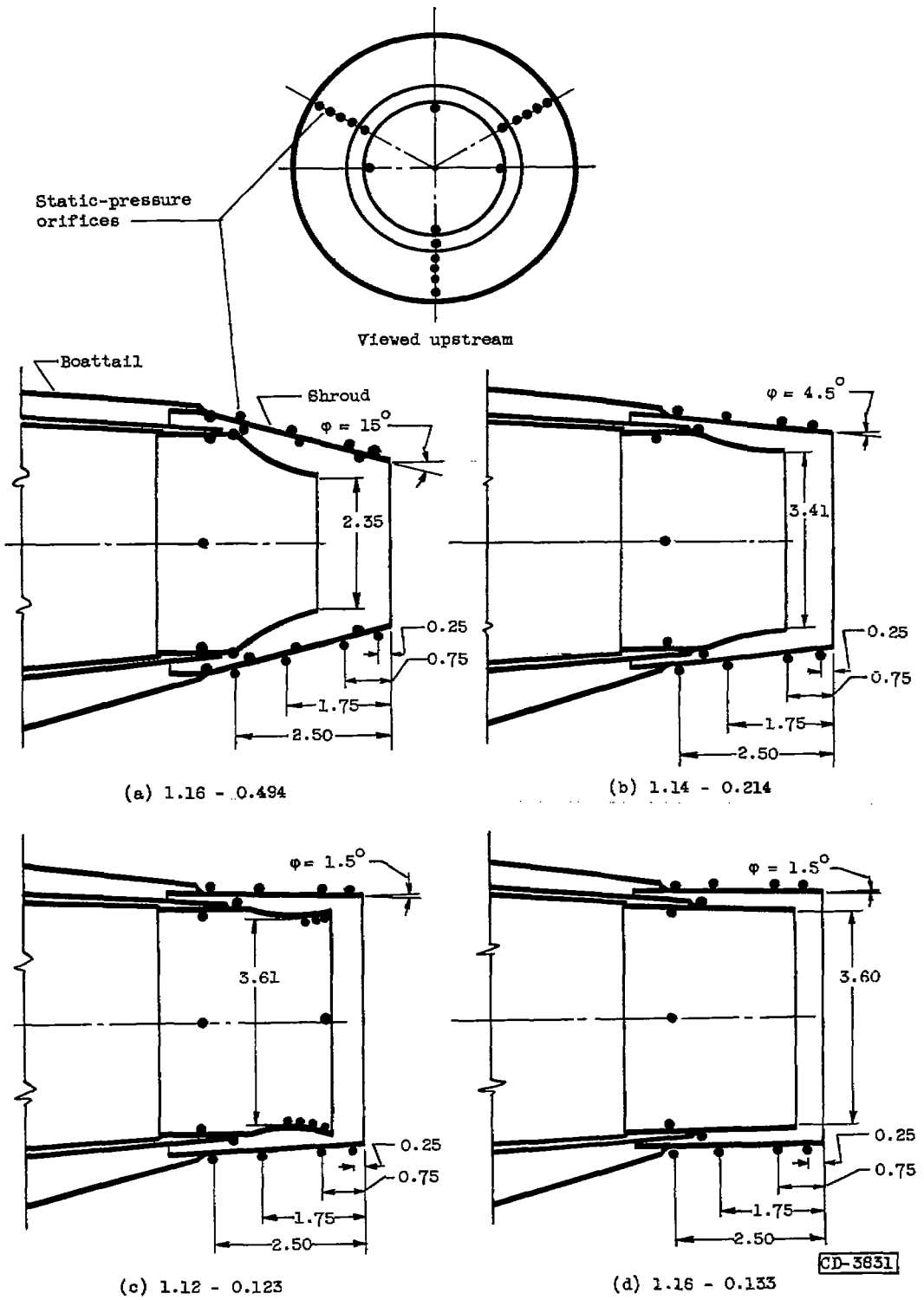

Figure 3. - Exit configurations with long shrouds showing pressure instrumentation. (All dimensions in inches.)

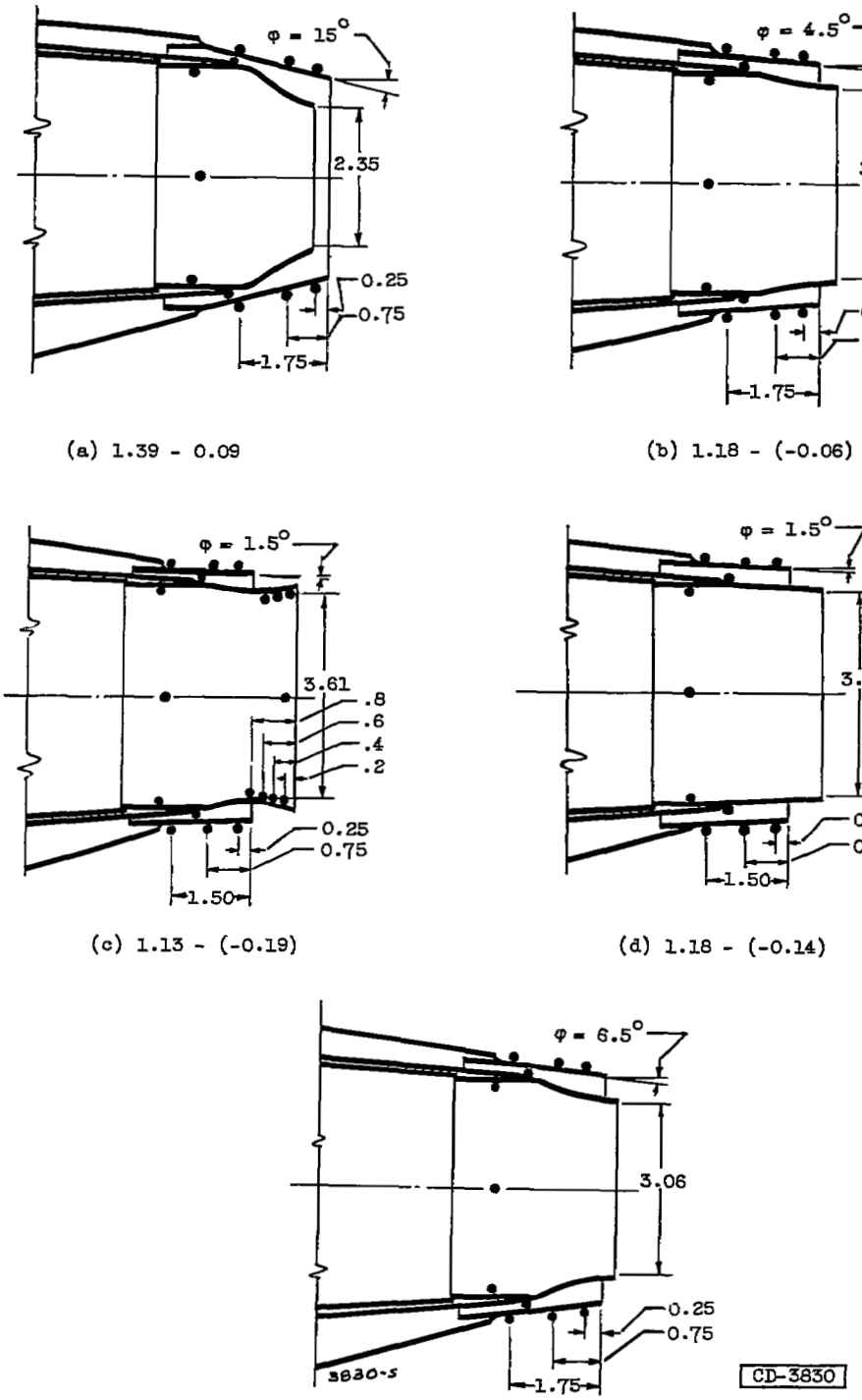

(a) 1.39 - 0.09

(b) 1.18 - (-0.06)

(c) 1.13 - (-0.19)

(d) 1.18 - (-0.14)

(e) 1.25 - (-0.10)

Figure 4. - Exit configurations with short shrouds showing pressure instrumentation. (All dimensions in inches.)

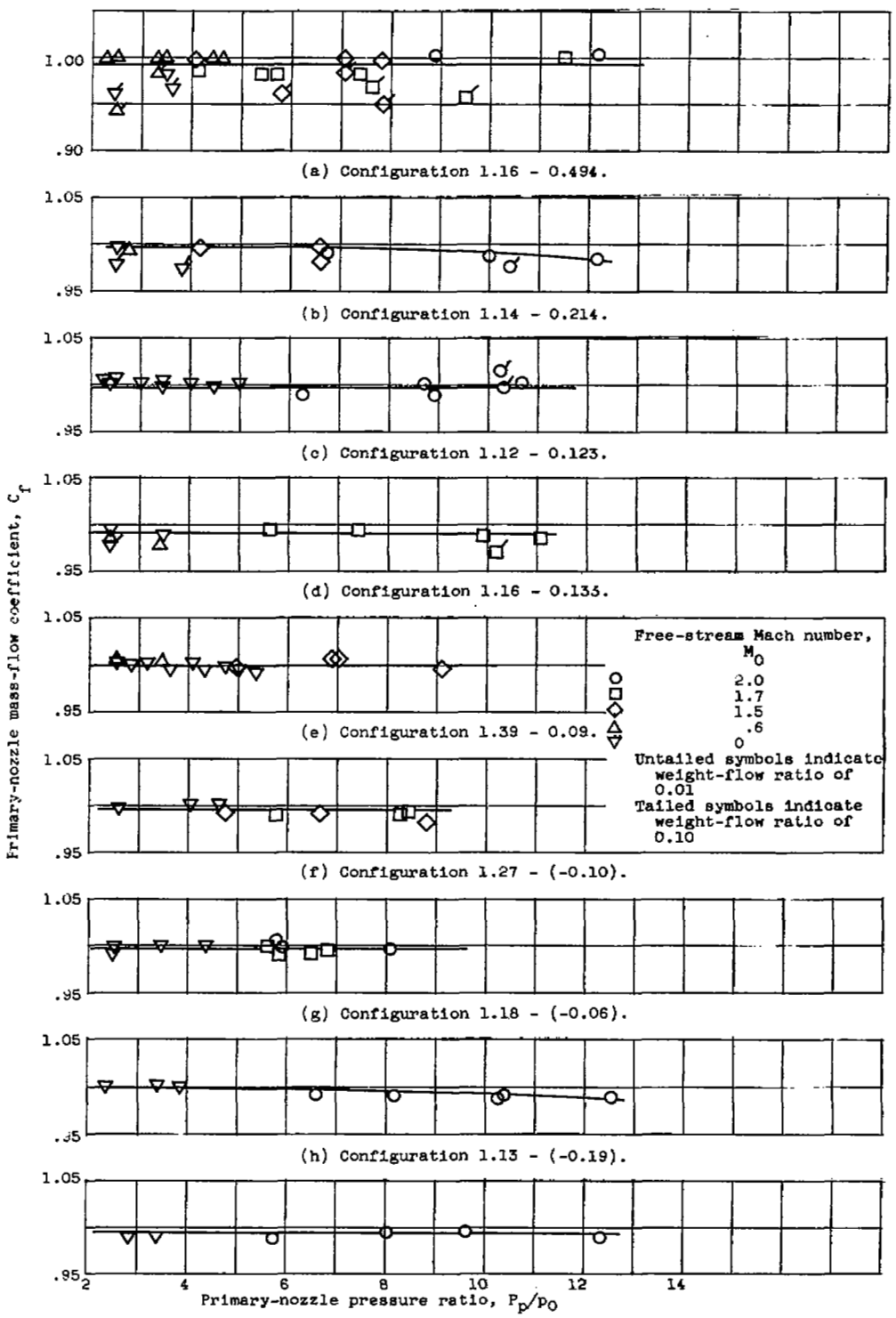

Figure 5. - Primary-nozzle mass-flow coefficients at zero angle of attack.

[redacted]

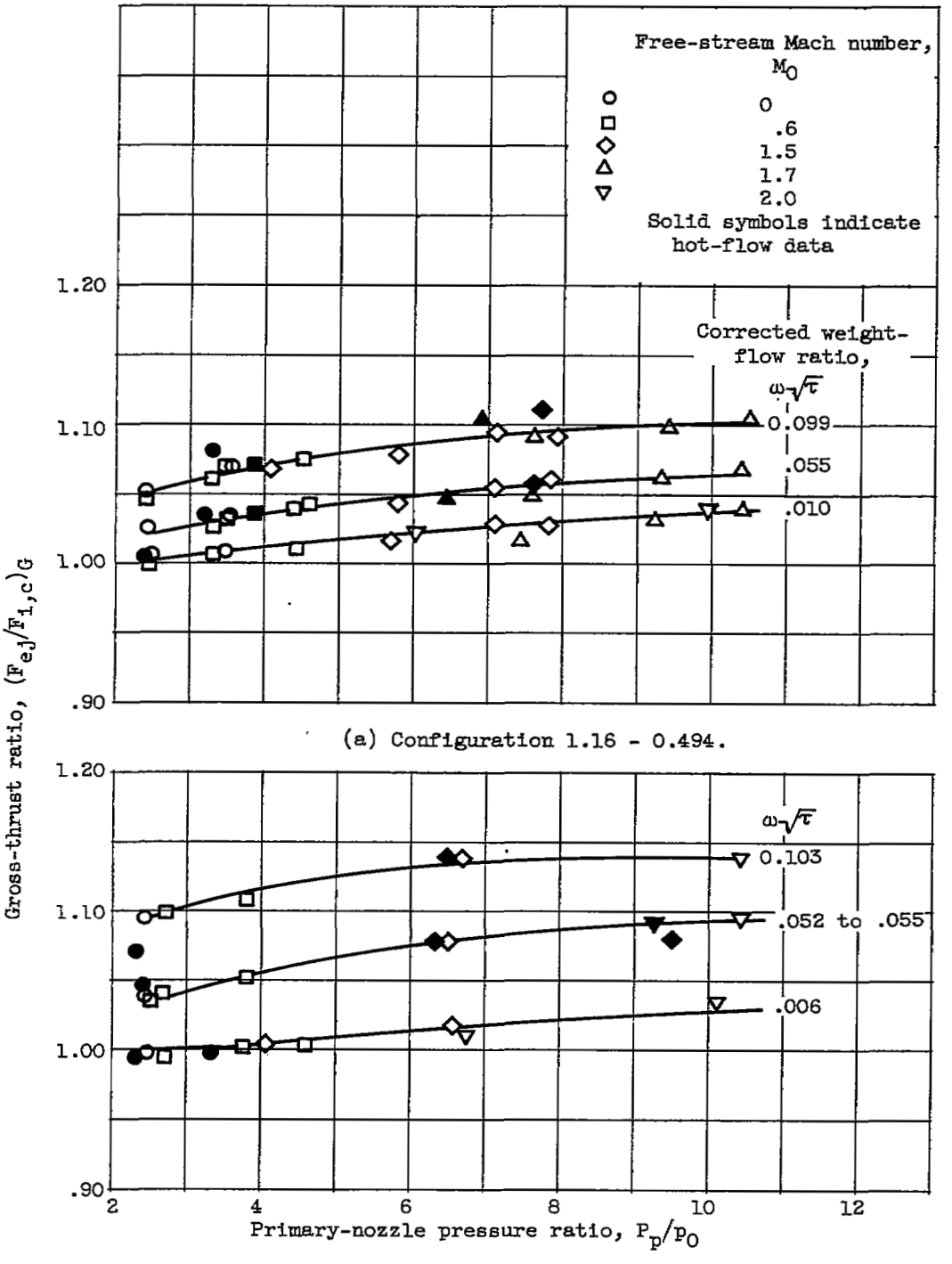

Figure 6. - Gross-thrust ratios of long-shroud nozzles at zero angle of attack.

[redacted]

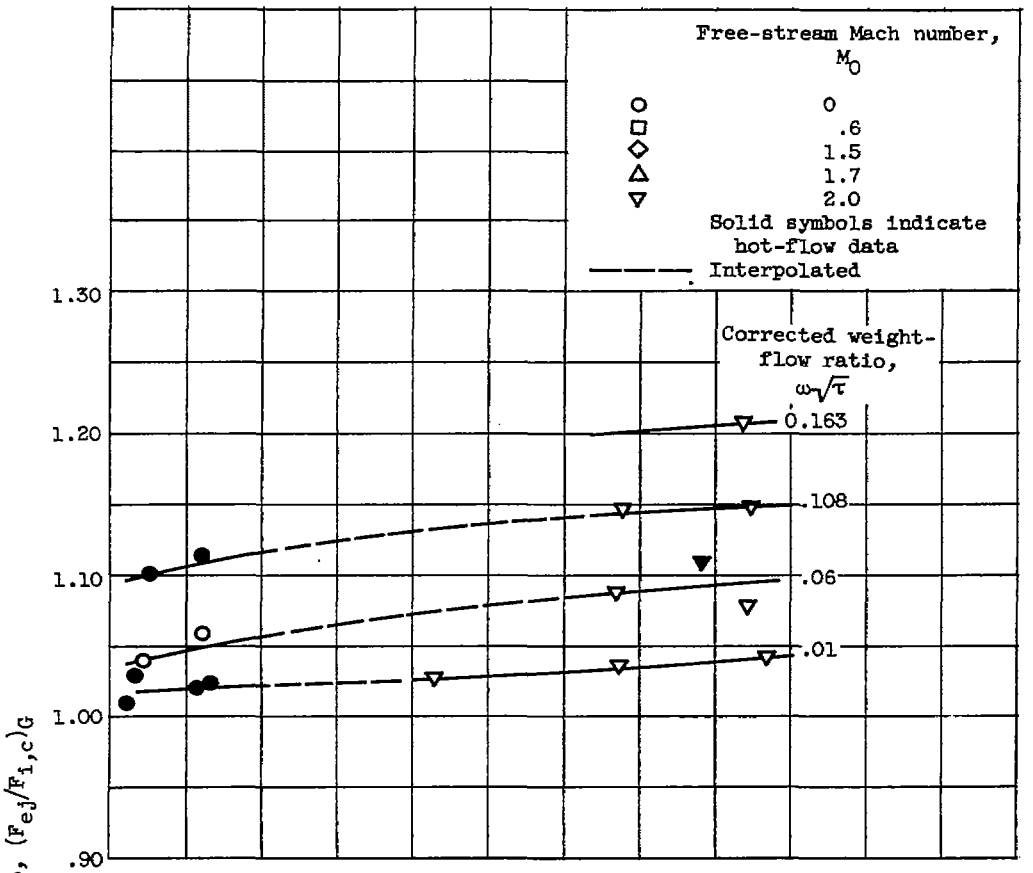

(c) Configuration 1.12 - 0.123.

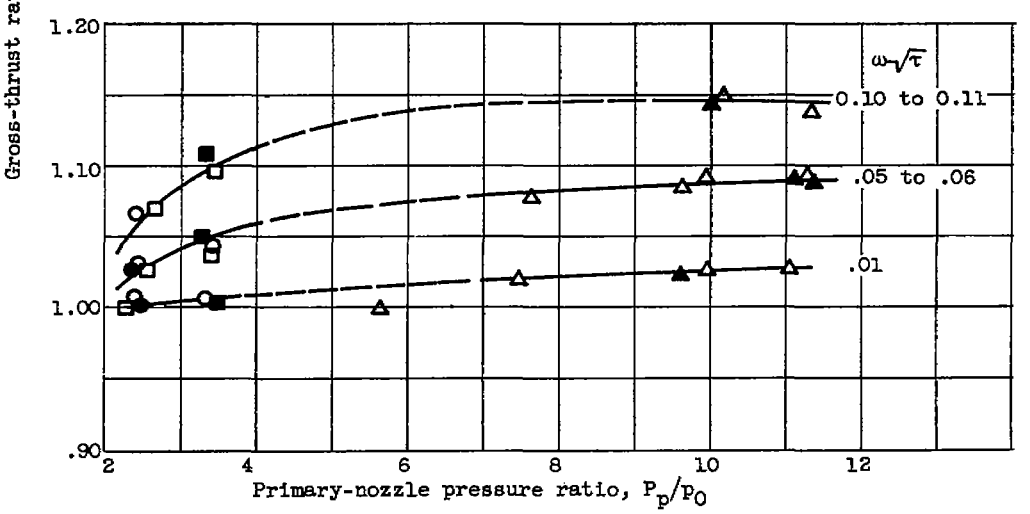

(d) Configuration 1.16 - 0.133.

Figure 6. - Concluded. Gross-thrust ratios of long-shroud nozzles at zero angle of attack.

[redacted]

3434

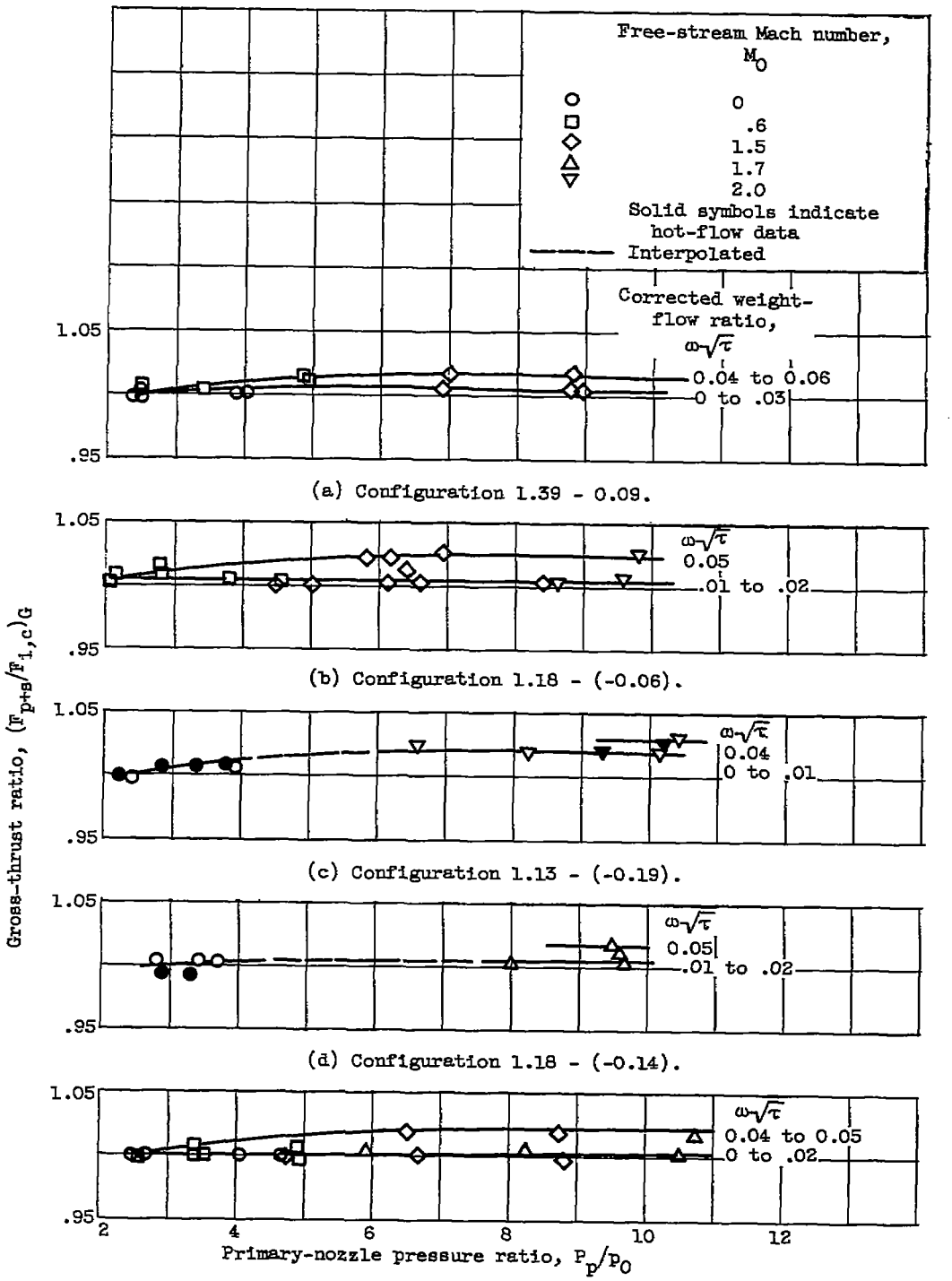

(a) Configuration 1.39 - 0.09.

(b) Configuration 1.18 - (-0.06).

(c) Configuration 1.13 - (-0.19).

(d) Configuration 1.18 - (-0.14).

(e) Configuration 1.27 - (-0.10).

Figure 7. - Gross-thrust ratios of short-shroud nozzles at zero angle of attack.

[redacted]

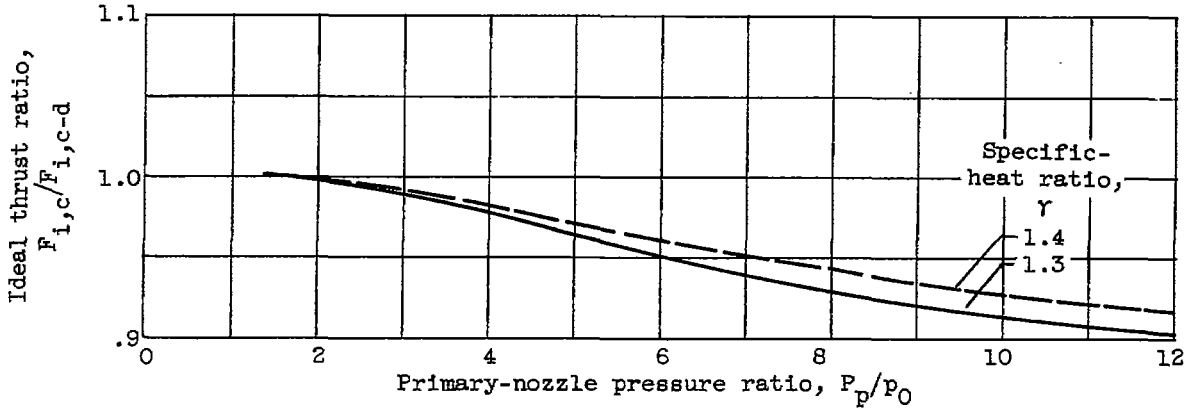

Figure 8. - Ratio of ideal thrust for sonic nozzle to that for nozzle expanded to free-stream static pressure.

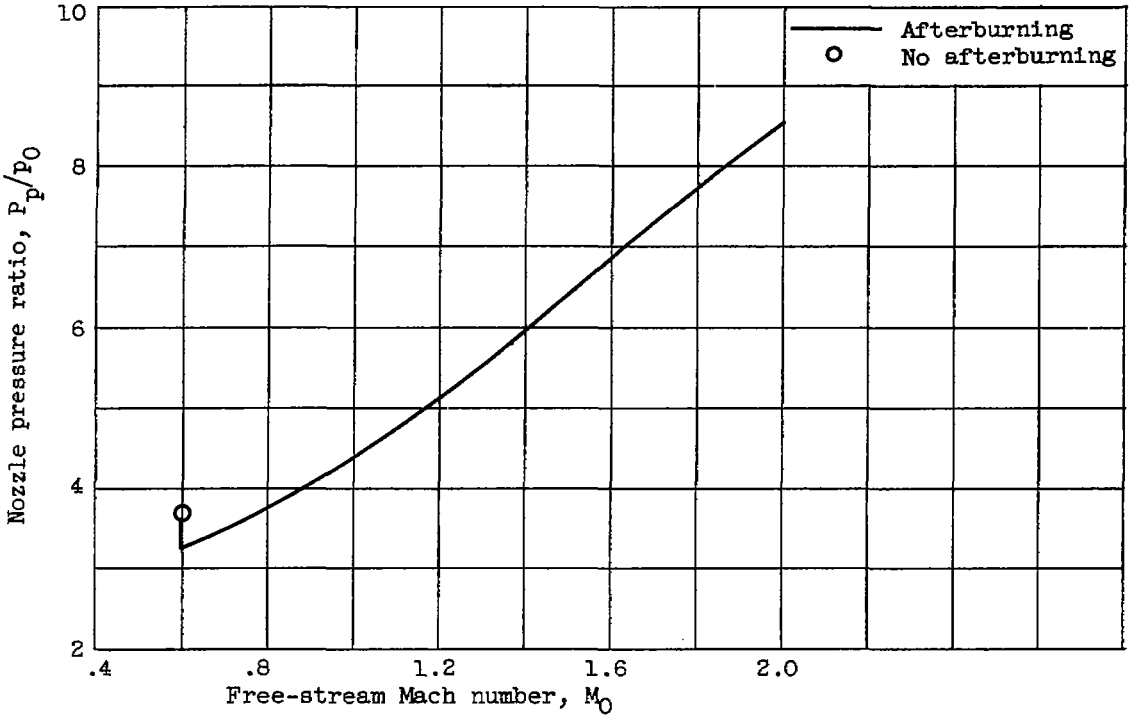

Figure 9. - Assumed primary-nozzle operating pressure ratios for a hypothetical turbojet engine with inlet diffuser losses included. Altitude, 35,000 ft.

3434

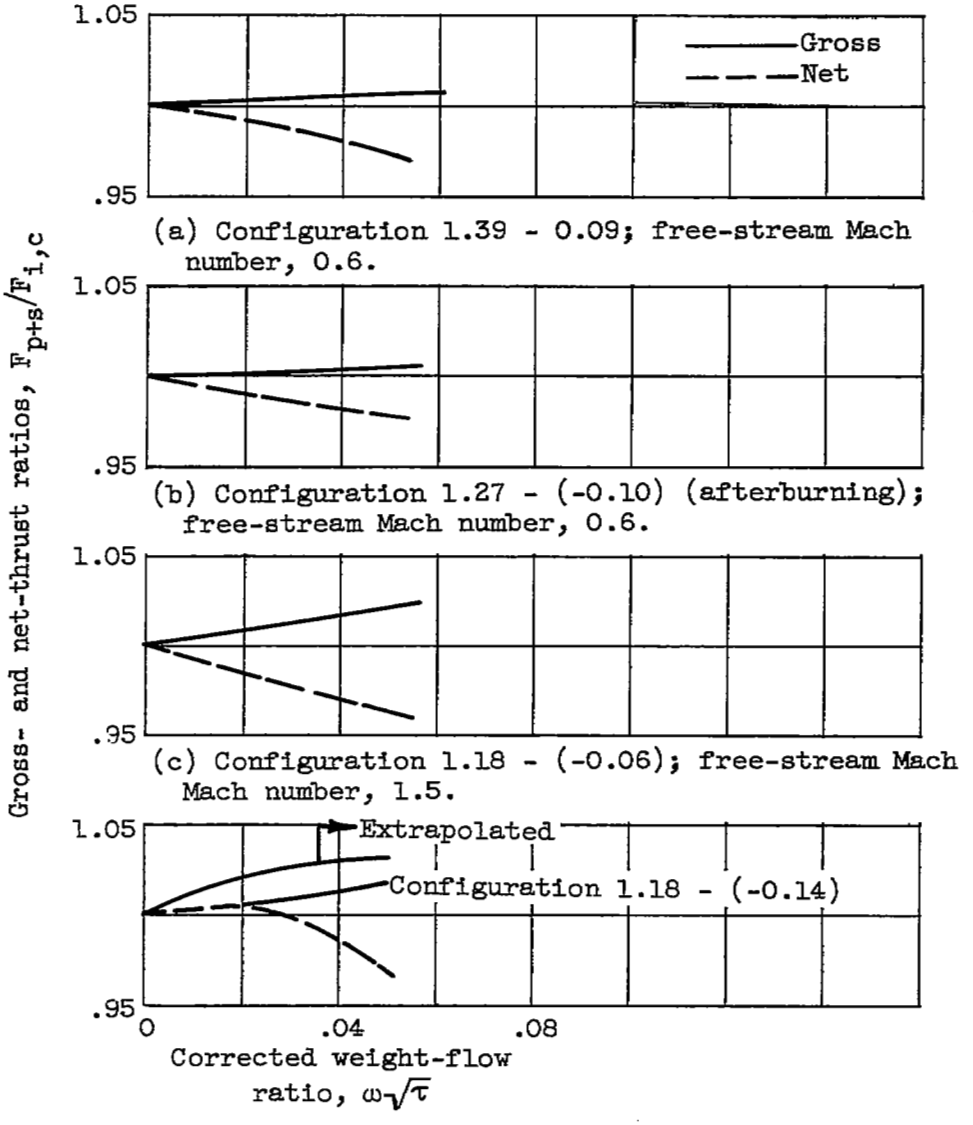

Figure 10. - Exit thrust performance at assumed nozzle operating pressure ratios of hypothetical turbojet engines. Short shrouds.

[redacted]

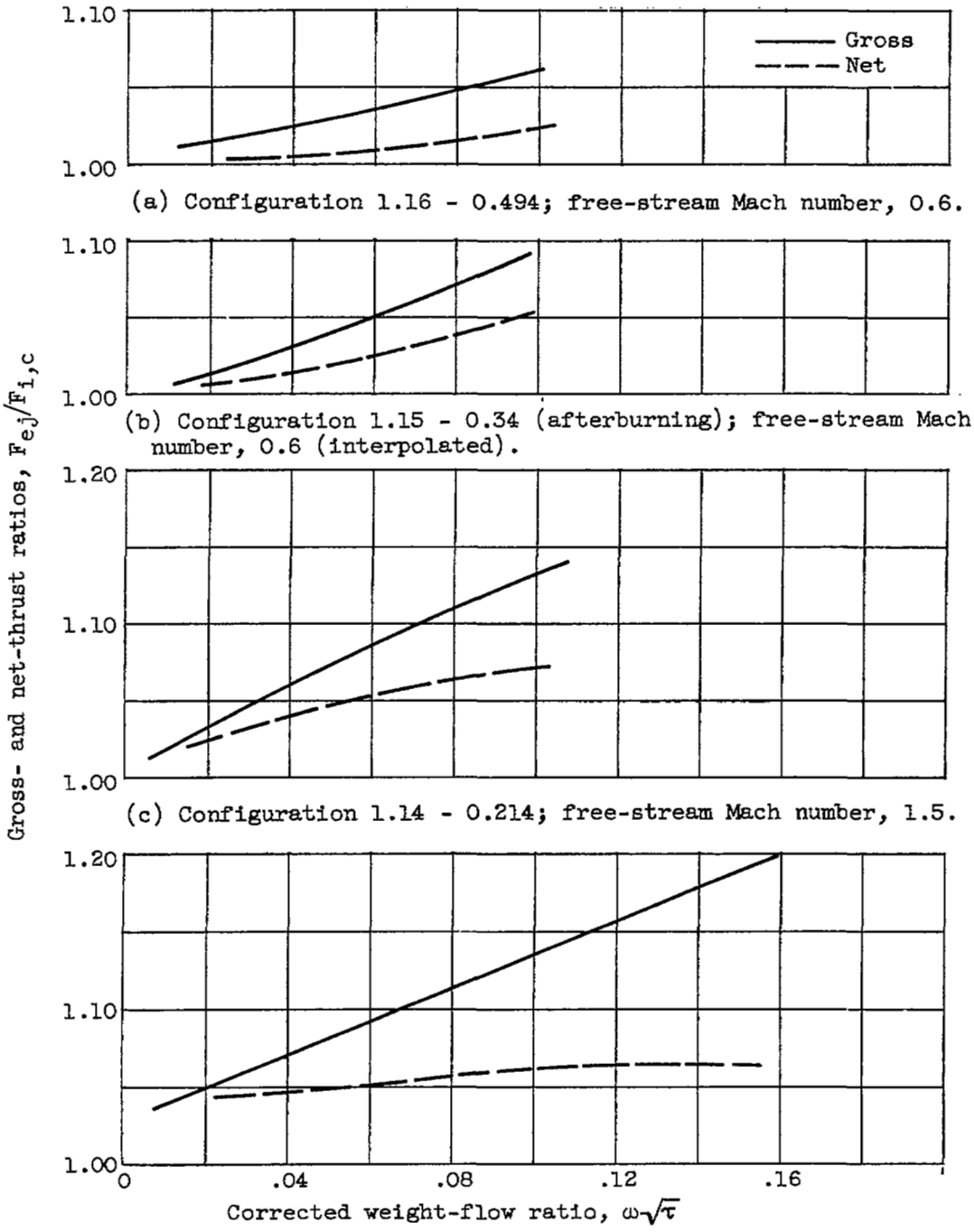

(a) Configuration 1.16 - 0.494; free-stream Mach number, 0.6.

(b) Configuration 1.15 - 0.34 (afterburning); free-stream Mach number, 0.6 (interpolated).

(c) Configuration 1.14 - 0.214; free-stream Mach number, 1.5.

(d) Configuration 1.12 - 0.123; free-stream Mach number, 2.0.

Figure 11. - Exit thrust performance at assumed nozzle operating pressure ratios of hypothetical turbojet engine. Long shrouds.

[redacted]

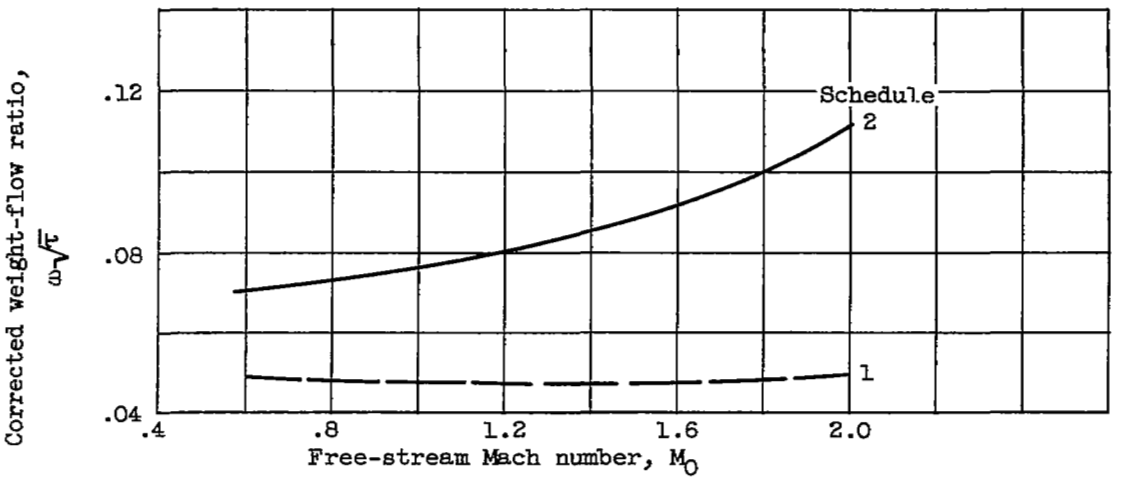

Figure 12. - Assumed schedule of secondary weight-flow ratios.

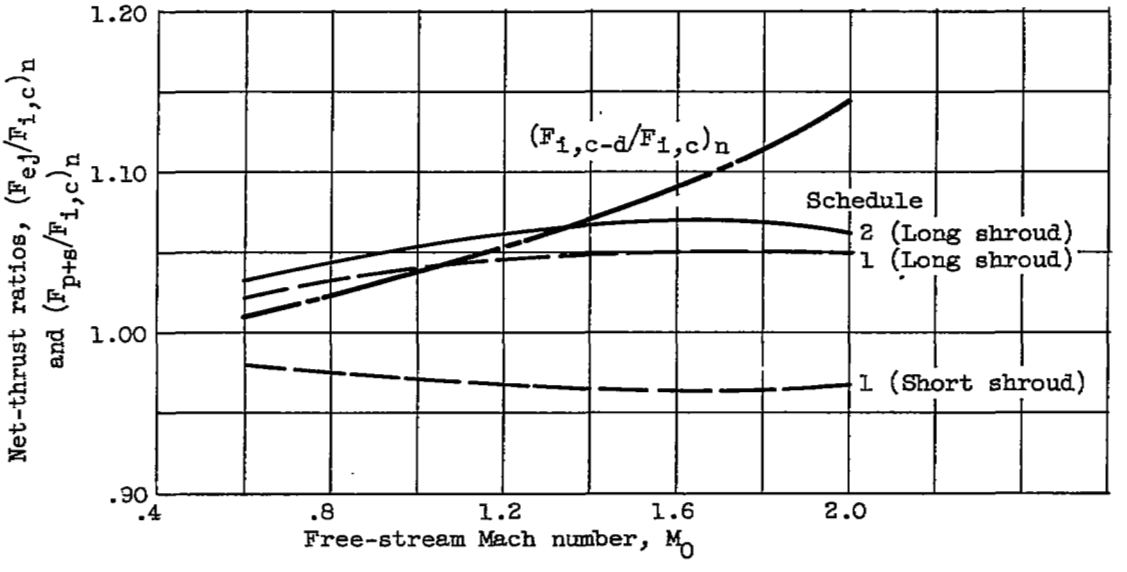

Figure 13. - Net-thrust comparisons of long- and short-shroud configurations. Altitude, 35,000 feet.

[redacted]

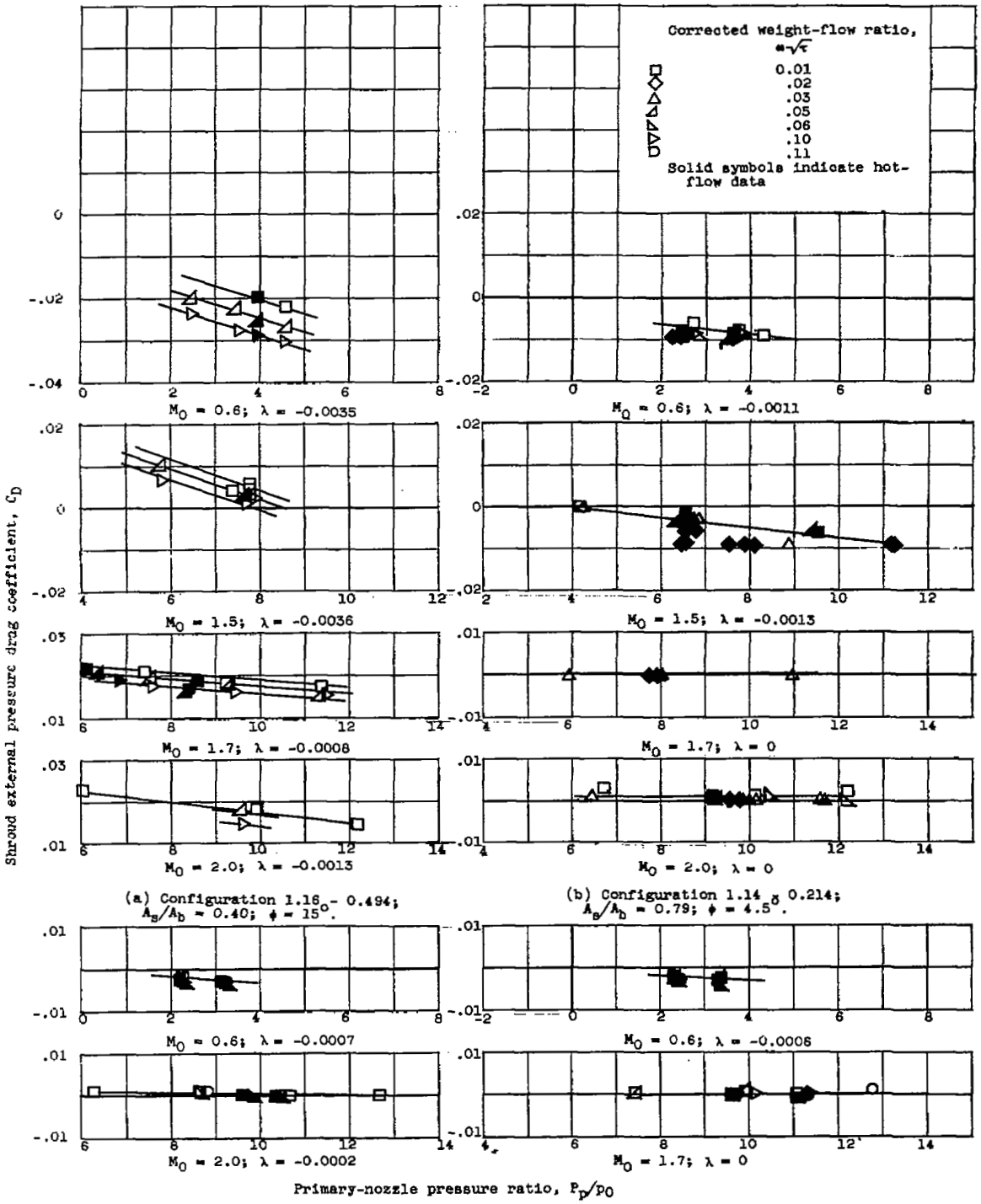

(a) Configuration 1.16$_0$ - 0.494; A_s/A_b = 0.40; ϕ = 15°.

(b) Configuration 1.14 $_\delta$ 0.214; A_s/A_b = 0.79; ϕ = 4.5°.

(c) Configuration 1.12 - 0.123; A_s/A_b = 0.93; ϕ = 1.5°.

(d) Configuration 1.16 - 0.133; A_s/A_b = 0.93; ϕ = 1.5°.

Figure 14. - Shroud external pressure drag coefficients of long-shroud nozzles.

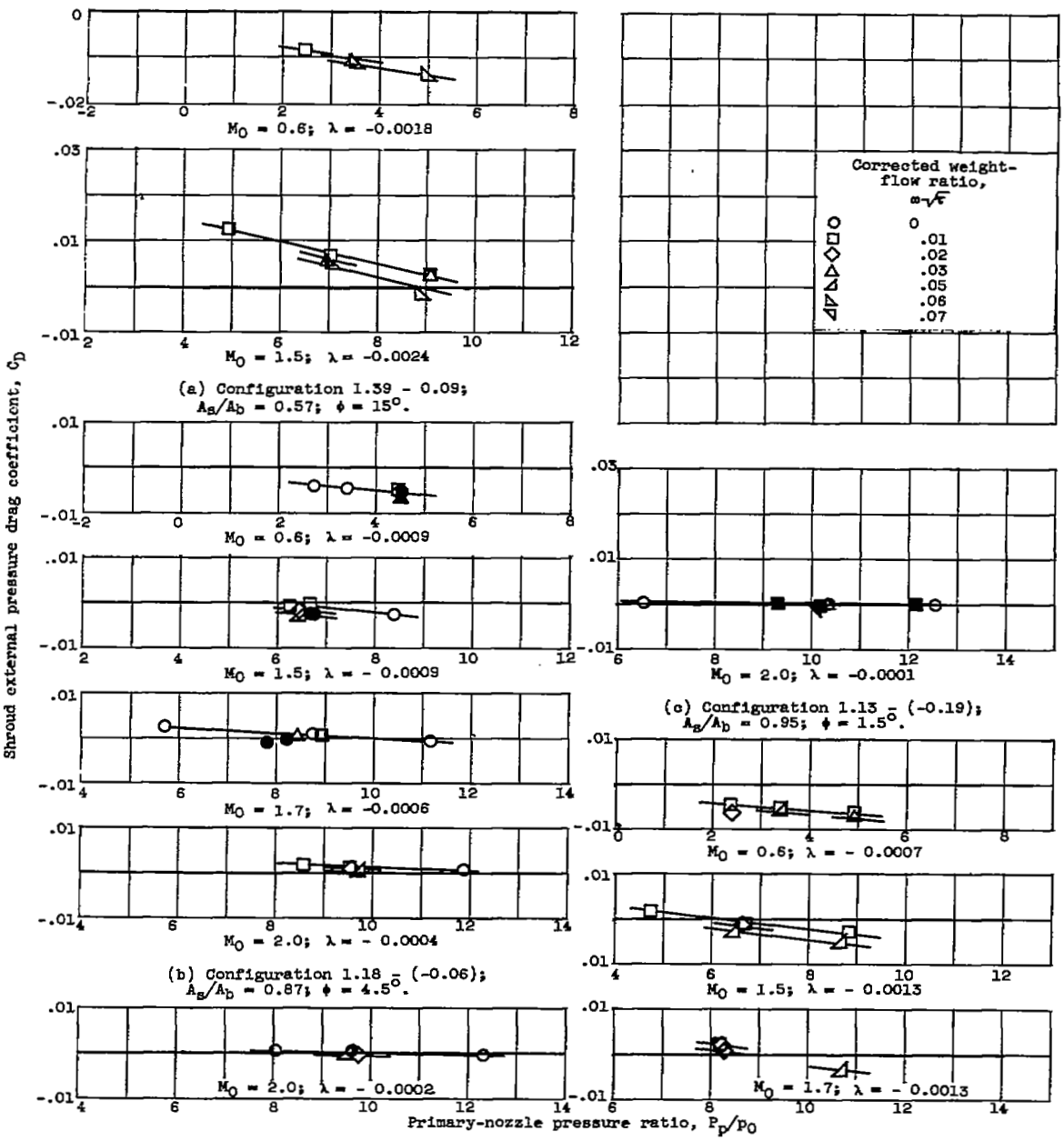

(a) Configuration 1.39 - 0.09; A_s/A_b = 0.57; ϕ = 15°.

(b) Configuration 1.18 - (-0.06); A_s/A_b = 0.87; ϕ = 4.5°.

(c) Configuration 1.13 - (-0.19); A_s/A_b = 0.95; ϕ = 1.5°.

(d) Configuration 1.18 - (-0.14); A_s/A_b = 0.95; ϕ = 1.5°.

(e) Configuration 1.27 - (-0.10); A_s/A_b = 0.80; ϕ = 6.5°.

Figure 15. - Shroud external pressure drag coefficients of short-shroud nozzles.

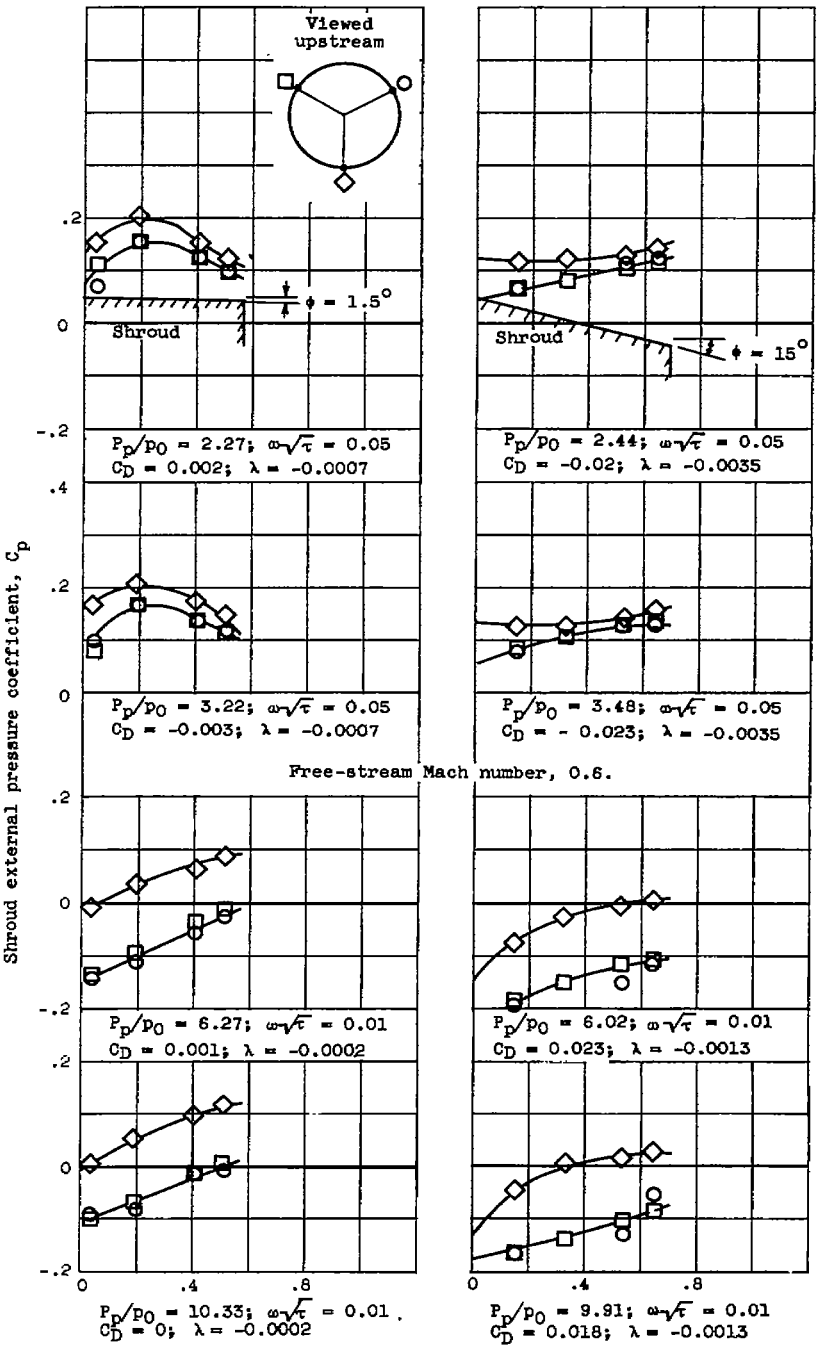

(a) Configuration 1.12 - 0.123; ϕ = 1.5°; A_s/A_b = 0.93.

(b) Configuration 1.16 - 0.494; ϕ = 15°; A_s/A_b = 0.40.

Figure 16. - Shroud pressure distribution for two configurations at free-stream Mach numbers of 0.6 and 2.0.

[redacted]

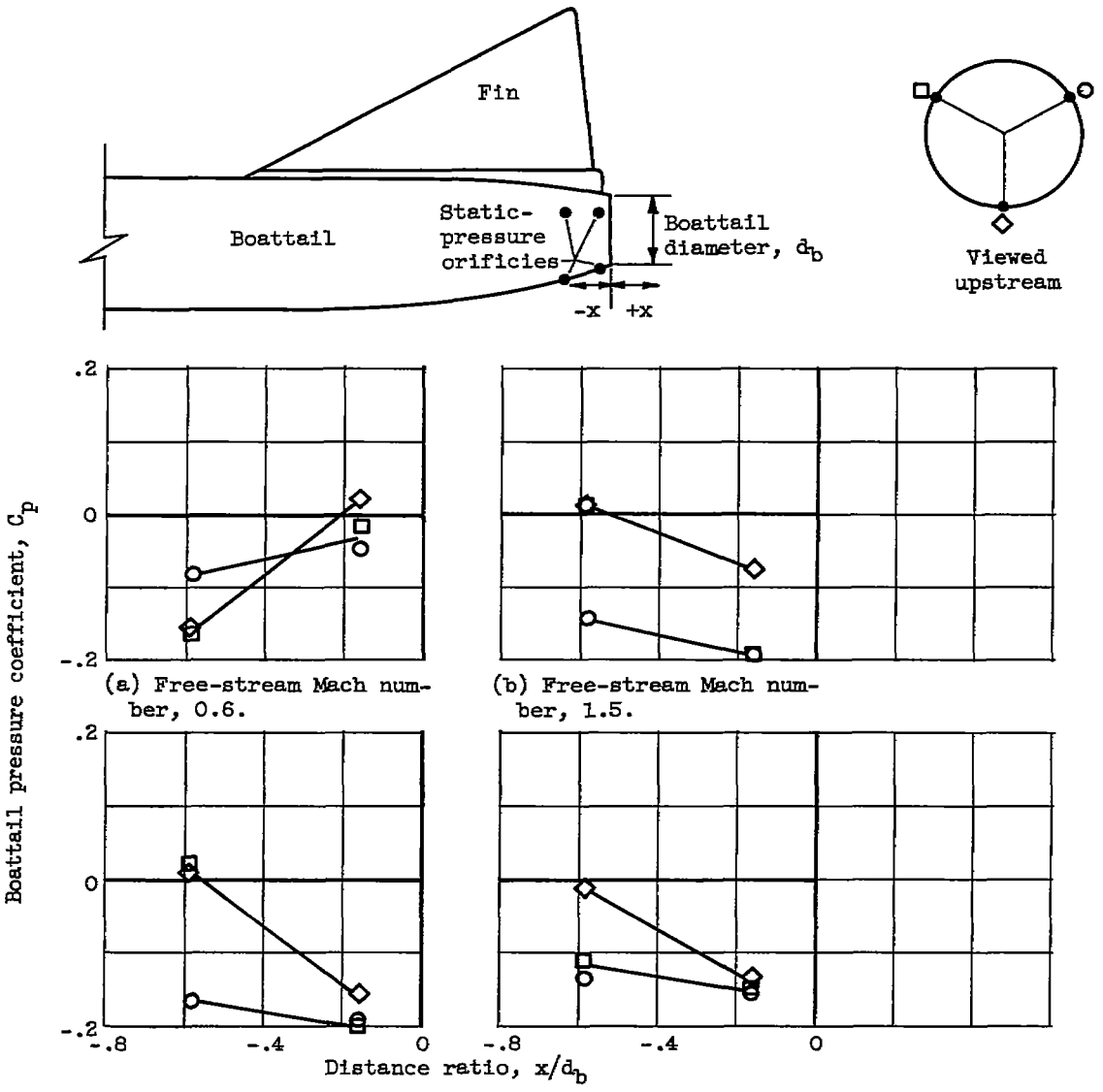

Figure 17. - Pressure coefficients on aft portion of boattail for model without shroud or nozzle and with base covered.